Preprint Title Investigation on drag reduction performance of pipeline with bioinspired microgrooved surface

Authors Weili Liu, Hongjian Ni, Peng Wang and Yi Zhou

Article Type Full Research Paper

ORCID® iDs Hongjian Ni - https://orcid.org/0000-0002-3467-1262

Investigation on drag reduction performance of pipeline with bioinspired microgrooved surface

Weili Liu[1,2,3], Hongjian Ni[*1,2], Peng Wang[1,2] and Yi Zhou[1,2]

Address: [1] School of Petroleum Engineering, China University of Petroleum (East China), Qingdao 266580, China, [2] Key Laboratory of Unconventional Oil & Gas Development (China University of Petroleum (East China)), Ministry of Education, Qingdao 266580, China and [3] Department of Chemical and Petroleum Engineering, University of Calgary, Calgary T2N1N4, Canada

Email: Hongjian Ni – hjn_upc@hotmail.com

* Corresponding author

ABSTRACT

Novel surface morphology of pipeline with transverse microgrooves was proposed for reducing the pressure loss of fluid transport. Numerical simulation and experimental research efforts were undertaken to evaluate the drag reduction performance of bionic pipeline. The computational fluid dynamic calculation, using SST κ-ω turbulent model, shown that the “vortex cushioning effect” and “driving effect” produced by the vortexes in the microgrooves were the main reason for the drag reduction. The shear stress of the microgrooved surface was reduced significantly owing to the decline of the velocity gradient; then bionic pipeline achieved drag reduction effect in the pipe and concentric annulus flow. The primary and secondary order of effect on the drag reduction and optimal microgroove geometric parameters were obtained by orthogonal analysis method. The comparative experiments were conducted in a water tunnel, and a maximum drag reduction rate of 3.21% was achieved. The numerical simulation and

experimental results were cross-checked and consistent with each other to verify that the utilization of bionic theory to reduce the pressure loss of fluid transport is feasible. Results can provide theoretical guidance for the energy saving of pipeline transportation.

Keywords

Fluid transport; Bionic pipeline; Drag reduction; Transverse microgrooves; Drag reduction mechanism.

Abbreviations

CFD	Computational fluid dynamic	DNS	Direct numerical simulation
RANS	Reynolds Averaged Navier-Stokes	Re	Reynolds number
DRR	Drag reduction rate		

Introduction

It is extremely urgent to improve energy efficiency with the gradual emergence of the energy crisis [1]. Drag reduction is important for vehicles and fluid transport to increase cruising speed and decrease the consumption of energy. In pipeline transportation, the transport drag is all from skin-friction drag, which is the main reason for affecting the transport efficiency of long-distance pipelines [2]. In drilling engineering, the high pressure loss is mainly caused by the skin-friction drag of the circulating drilling fluid, which severely hinders the progress of oil and gas resources exploration of deep well [3-5]. Therefore, it is necessary to put more effects into reducing the skin-friction drag. Conventional hydraulic drag reduction methods include developing high-performance

polymer additives to reduce fluid viscosity [7-9], injecting gas to modify the turbulent boundary characteristics [10], fabricating superhydrophobic surface to reduce the adhesion [11]. However, the application of polymer additives is not economic and anti-drag performance of additives is also instability in some complex conditions. Besides, these active anti-drag methods require extra energy or complicate the services, which limits their engineering application.

Pressure loss mainly derives from the shear stress of fluid flowing through the surface of the pipeline. The wall shear stress is described as:

$$\tau = \mu \frac{du}{dy} \qquad (1)$$

Where τ, is the shear stress (Pa), μ is the dynamic viscosity of fluid (Pa·s); du/dy is the velocity gradient (1/s). According to Eq. 1, changing the turbulent boundary layer state of vicinity wall for decreasing velocity gradient is an essential and appropriate measure to reduce drag [12]. Bionic research found that some natural organisms have formed a specific surface structure with anti-drag [13], anti-wear [14,15] and hydrophobic [16,17] performance in the evolution of billions of years for adapting to the living environment. Bionic theories have been applied to many engineering fields, such as microstructured tunnel in the external flow [18] and internal flow [19], bionic pump cylinder liner [20], and bionic bearing slider [21], which settle lots of practical problems. An inspiration for a drag reduction surface is provided by the skin of sharks and the feather of birds [13,22]. As shown in Figure 1, the microgrooves are the crucial factor to experience low drag and fast speed for the sharks and birds. From the perspective

of the urgent demand for decreasing pressure loss of fluid transport and the practical value of bionic theory, the bionic microstructure can be applied to the pipeline surface [23,24]. It provides a novel improving method for pipeline, and potential for anti-drag and anti-wear performance may be achieved by bionic drill pipe in the drilling engineering.

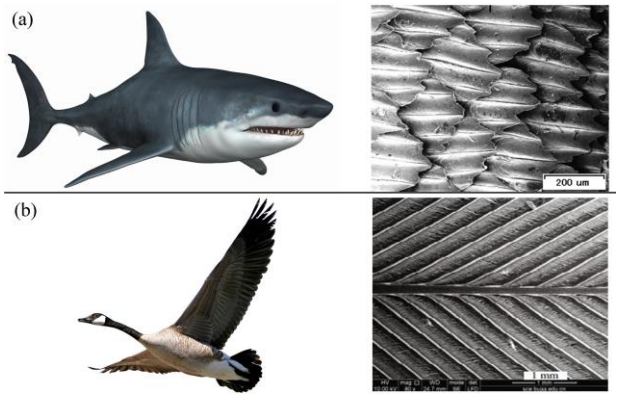

Figure 1: SEM photo of (a) shark skin and (b) bird feather.

In the last decades, utilizing bionic microstructures to reduce the drag of turbulent flow has become a research hotspot. This technique has a remarkable effect on energy saving in engineering applications [25,26], such as fuel pipelines, aircraft, vehicles. Furthermore, as a passive and portable drag reduction technique, it needs no extra energy. According to the configuration direction of bionic microstructure, it can be divided into streamwise grooves and transverse grooves. With the development of numerical simulation and experimental techniques, the influence of microstructures on turbulent flow characteristics is investigated accurately. Its drag reduction mechanism owes to two aspects of reducing viscous drag and controlling boundary layer separation [27, 28]. By imitating the microgrooves of sharkskin, the drag reduction

performance of streamwise grooves has been validated by many researchers both in external flat and internal rectangular duct turbulent flow [18,19,22,29-32]. The biggest drag reduction rate (DRR) can be up to 10%.

Comparatively, research on drag reduction of transverse microgroove started late, and its drag reduction performance is controversial. Walsh [33] measured the drag of convex transverse groove in external flat flow, and a slight increase drag date is found. Tokunaga [34] investigated turbulent channel flow with one concave transverse groove by LES method, and the results show that the turbulent is weakened and substantial drag reduction is found at the Reynolds number 8,000. Dou et al. [35] mimicked fish scales to fabricate bionic surface through coating technology, and obtain remarkable drag reduction performance in a water tunnel experiment. Feng et al. [13] mimicked bird feather to fabricate a bionic surface with transverse grooves through hot-rolling technology, and obtain significant drag reduction efficiency in a wind tunnel experiment. Mariotti et al. [36] assessed the drag reduction performance of boat-tailed axisymmetric bodies with transverse grooves, with a consequence of significant DRR owing to the delay of boundary layer separation.

From the above analysis we can know that most of the previous studies focused on external flow with bionic microstructure, however, there are few studies on the internal flow of pipeline with transverse microgrooves [35]. Therefore, it is necessary to evaluate the drag reduction performance of transverse microgrooves in the internal pipe flow, which can provide theoretical guidance for the energy saving of fluid pipeline

transportation.

In this study, the drag reduction performance of bionic pipeline in the pipe flow and the concentric annulus flow was investigated. Firstly, computational fluid dynamic (CFD) method was used to analyze the hydraulic characteristics of pipeline inner surface and outer surface with transverse microgrooves, respectively. Besides, the influence of microgroove geometric parameters on the turbulent flow field and microgrooves structure optimization were obtained. Then comparative experiments between microgrooved pipeline outer surface and smooth surface were conducted in a water tunnel annular flow to evaluate the drag reduction performance of transverse microgrooves. Finally, the drag reduction mechanism of transverse microgrooves was revealed systematically.

Methods

CFD simulation method and validation

Physical models

Pressure loss mainly derives from fluid turbulent flow in the pipeline and the annulus between coaxial pipelines, so the inner wall and outer wall of pipeline with transverse microgrooves need to be modeled, respectively. In order to reduce computational workload, the two-dimensional axisymmetric models were used to simulate the pipe flow and concentric annulus flow. The annulus inner diameter and outer diameter were set to 20 mm and 34 mm, respectively. The hydraulic diameter of the pipe and annulus D = 14 mm, according to the suggestion of Eggles [37], the flow direction length of

model L = 5D = 70 mm. The physical models of pipe flow and annulus flow formed by two coaxial pipelines are shown in Figure 2, transverse microgrooves with triangular section evenly distributed on the surface of the pipeline. The model of smooth wall with the same size of diameter and length was also established for comparing the flow drag with the bionic pipeline under the same condition.

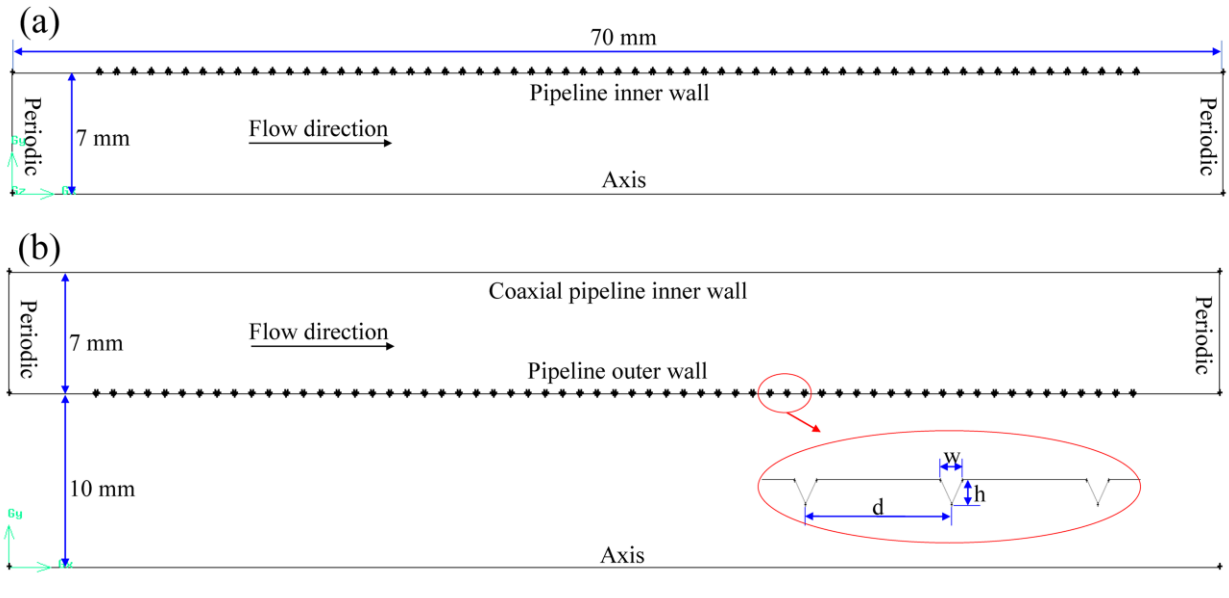

Figure 2: Physical models. (a) Pipe flow model with transverse microgrooves. (b) Concentric annulus flow model with transverse microgrooves.

Governing equations

A commercial CFD tool of ANSYS Fluent-18.0 was implemented to calculate the turbulent flow in the pipe and concentric annulus. Near-wall turbulence characteristics of a drag reducing polymer fluid flow in concentric annulus was successfully simulated with SST κ-ω model [38]. Besides, the SST model combines the advantages of κ-ε model the near-wall and κ-ω model away from the wall, which reducing the influence of wall grid density on computational accuracy. Taking into account computational accuracy and computational cost, the Reynolds Averaged Navier-Stokes (RANS)

numerical simulation method with the SST turbulence model was adopted to analyze the hydraulic characteristics of near-wall turbulent flow. The governing equations are as follows:

Continuity equation:

$$\frac{\partial(\rho u_i)}{\partial x_i} = 0 \qquad (2)$$

Momentum equation：

$$\frac{\partial}{\partial x_j}\left(\rho u_i u_j\right) = -\frac{\partial P}{\partial x_i} + \frac{\partial}{\partial x_j}\left(\mu\frac{\partial u_i}{\partial x_j} - \rho\overline{u_i' u_j'}\right) \qquad (3)$$

κ equation：

$$\frac{\partial}{\partial t}(\rho k) + \frac{\partial}{\partial x_i}(\rho k u_i) = \frac{\partial}{\partial x_j}\left(\Gamma_k\frac{\partial k}{\partial x_j}\right) + G_k$$

$$-Y_k + S_k \qquad (4)$$

ω equation：

$$\frac{\partial}{\partial t}(\rho\omega) + \frac{\partial}{\partial x_i}(\rho\omega u_i) = \frac{\partial}{\partial x_j}\left(\Gamma_\omega\frac{\partial \omega}{\partial x_j}\right) + G_\omega$$

$$-Y_\omega + D_\omega + S_\omega \qquad (5)$$

where i, j are coordinate direction and direction of the velocity components, respectively, $i = 1,2,3$, $j = 1,2,3$; u_i、u_j are the speed of different coordinate directions (m/s); ρ is the density of fluid (kg/m^3); $-\rho\overline{u_i' u_j'}$ is Reynolds stress; G_k is turbulent kinetic energy produced by a velocity gradient; G_ω is generated by the ω equation; Γ_k, Γ_ω are effective diffusion terms of *k* and ω, respectively; Y_k, Y_ω are turbulence generated by diffusion, respectively; D_ω, is orthogonal divergence term; S_k, S_ω are user-defined terms, respectively.

Boundary conditions and other parameters setting

In order to compare the hydraulic characteristics of grooved and smooth pipeline, exclude the effect of other factors on simulation results, simulation calculations use the same parameter settings, the specific conditions were set as follows:

(1) The periodic boundary condition was adopted along the flow direction for guaranteeing the turbulent flow is fully developed; no-slip boundary condition was adopted for the wall (as shown in Figure 2). The desired velocity was achieved by adopting a steady mass flow boundary condition.

(2) Incompressible water was used as continuous phase medium, the density is 998.2 kg/m^3, and the dynamic viscosity is 0.001003 Pa·s.

(3) Pressure-velocity coupling scheme is SMIPLEC; momentum equation was discretized by second order upwind scheme to ensure accuracy and stability.

Independence validation of grid density

The finite volume method was used to discretize the computational domain to unstructured triangular grids. The grids of the grooved wall were refined, and the grids became coarse gradually as away from the wall by size function. Grid density would affect computational accuracy, so the influence of grid density on shear stress of smooth pipeline was analyzed. As can be seen from Figure 3, when the number of grid element exceeds 320000, the shear stress tends to be stable under different velocities. Therefore, the number of grid element should not be less than 320000 in the numerical simulation.

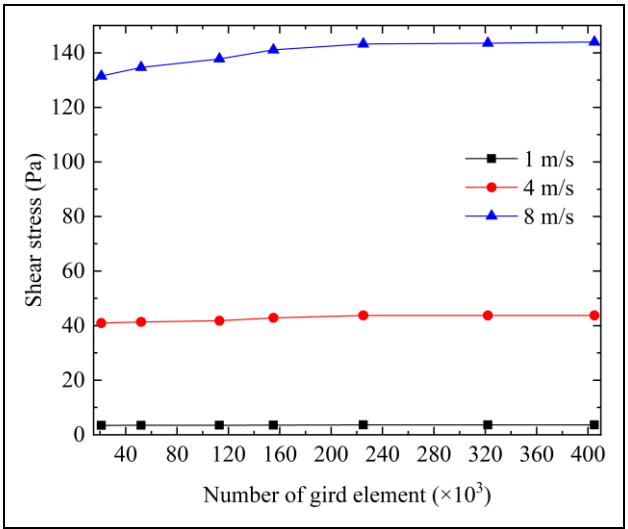

Figure 3: Influence of grid density on the viscous drag of pipe flow.

The smooth models and bionic models were meshed with the same meshing strategy to guarantee computational results are irrelevant to grid density. The grids with local amplification are depicted in Figure 4.

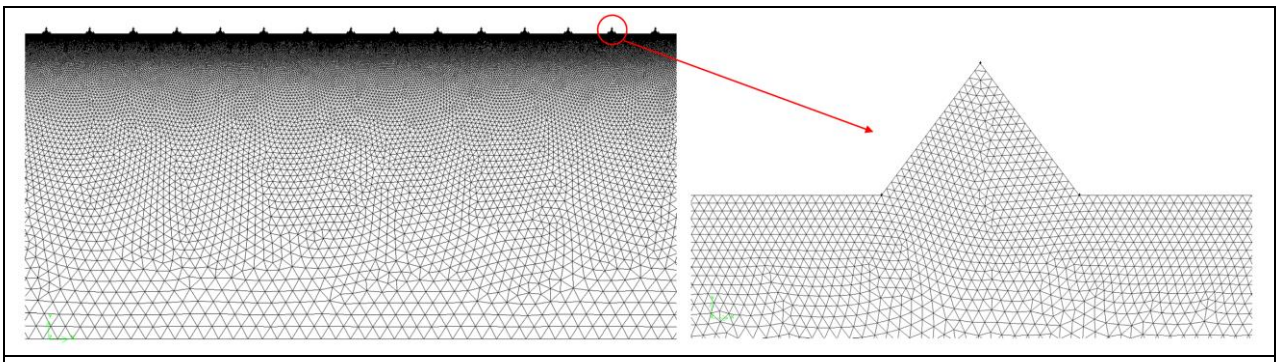

Figure 4: Computational grids of the bionic pipeline.

Validation of CFD results

Before analyzing turbulent flow, it is essential to validate the accuracy of numerical simulation methods.

(1) Validation of pipe flow

The simulated viscous coefficient of smooth pipeline was compared with the results of empirical formula by following methods:

Reynolds number: $Re = \frac{\rho U_m D}{\mu}$ (6)

The empirical formulas for viscous coefficient of smooth pipeline are as follows.

Braustian formula:

$f = 0.3164/Re^{0.25}$ $4000 < Re < 10^5$ (7)

Nikolaze formula:

$f = \frac{0.221}{Re^{0.237}} + 0.0032$ $10^5 < Re < 3\times10^6$ (8)

Numerical simulation for viscous coefficient of smooth pipeline:

$$f_{SST} = 8\tau/\rho V^2 \quad (9)$$

Where U_m is bulk velocity (m/s); D is hydraulic diameter (m); τ is shear stress (Pa), which is calculated by numerical simulation. As can be seen from the comparison dates in Table 1, the maximum relative error is within the allowable range, so the present numerical simulation method is reliable.

Table 1: Comparison of empirical and simulated viscous coefficients of pipe flow.

U_m(m/s)	*Re*	*f*	f_{SST}	Relative error(%)
1	13933	0.02912	0.02941	-1.01
5	69665	0.01948	0.02011	-3.18
10	139300	0.01654	0.01699	-2.72
20	278660	0.01452	0.01436	1.11

(2) Validation of annulus flow

Then the physical model of the annulus with identical boundary conditions as that of Chung et al. [39] was calculated by the present numerical simulation method. The velocity distributions of annulus flow were compared with direct numerical simulation (DNS) results, shown in Figure 5. The agreement with DNS is satisfactory, so the

accuracy of the numerical simulation method is validated again.

Parametric dimensionless:

$$u_\tau = \sqrt{\tau/\rho} \qquad (10)$$

$$U^+ = U/u_\tau \qquad (11)$$

$$y^+ = yu_\tau/v \qquad (12)$$

Where u_τ is friction velocity (m/s); U is instantaneous velocity (m/s); y is normal distance from wall (m); v is kinematic viscosity (m^2/s).

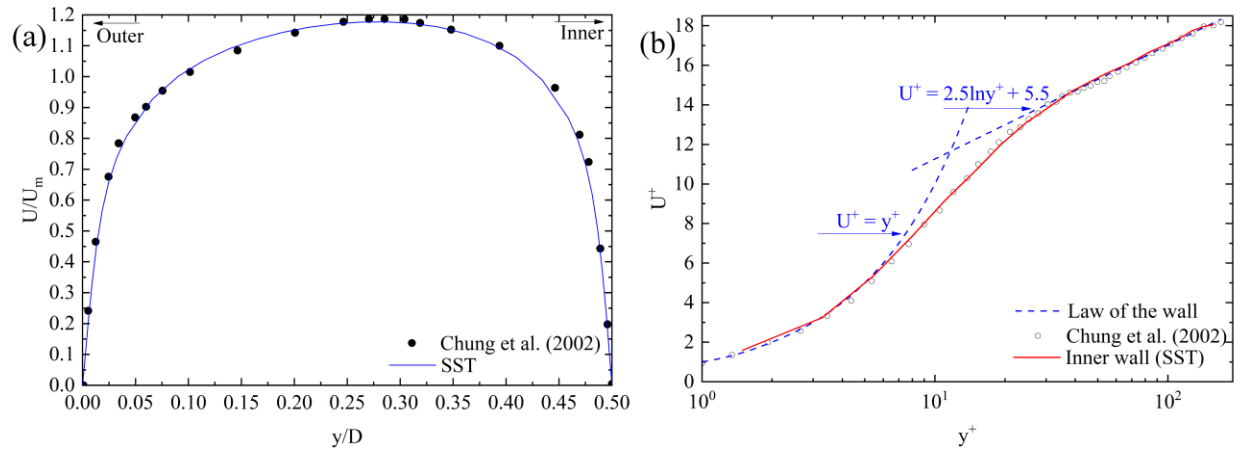

Figure 5: Comparison of SST results with DNS results. (a) Mean velocity distributions of the annulus flow. (b) Velocity distributions for the law of wall.

Drag reduction evaluation method

Under the same simulation conditions, the average drag of the smooth pipeline and the bionic pipeline were compared to obtain the DRR of transverse microgrooves, which can be defined as follows:

$$\eta = \frac{F_s - F_b}{F_s} \times 100\% \qquad (13)$$

Where η is DRR (%); F_s and F_b are the average drag of smooth surface and bionic surface (N), respectively; F_b includes viscous drag and pressure drag; When the DRR

is positive, it indicates that the transverse microgrooves have drag reduction effect.

Experimental method

Experimental set-up and procedure

The accuracy and reliability of numerical simulation results need experimental verification, so comparative experiments of bionic pipeline and smooth pipeline were carried out in a water tunnel. Figure 6 shows the pressure loss testing set-up of concentric annulus flow, the length of the test section is 2.2 m, the circulation medium is tap-water, and the rate of flow can be changed by the control valve. In the whole experimental procedure, the liquid level water tank 2 remains to overflow for guaranteeing the contrast experiment under the same water head height. In order to ensure that the test section is in a fully developed turbulent flow, the length of the annulus entrance section and export section is reserved with 0.5 m. The pressure loss of the annulus test section was measured by a high precision differential pressure transmitter, and the flow rate was measured by the weighing method.

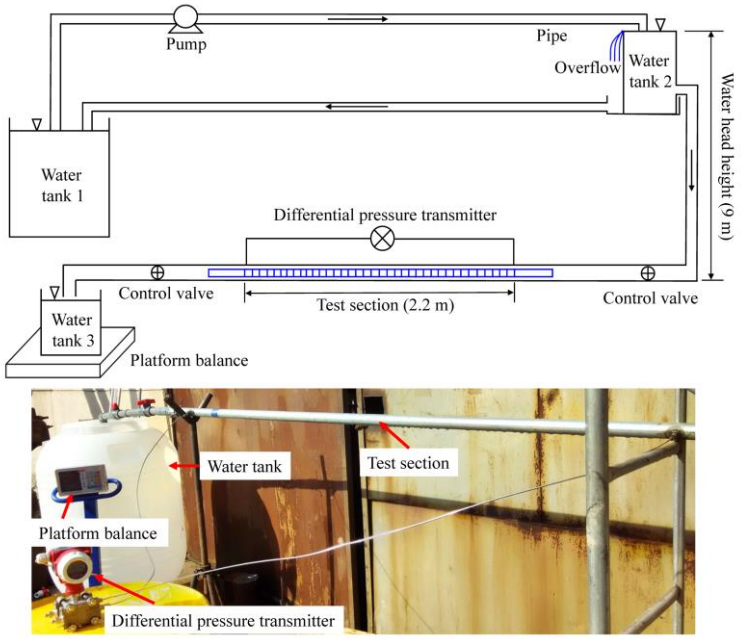

Figure 6: Schematic of the experimental set-up.

The experimental procedures are as follows. Firstly, installing scaled pipeline and adjusting its position to center it in the annulus. Then, gathering 30 groups of pressure drop value at intervals of 5 seconds to obtain the average value after the flow is stable. Thirdly, weighing the water of the water tank 3 collected in 120 seconds to calculate the flow rate. The average values of pressure loss and flow rate were measured by three repeated experiments under the same conditions to decrease measuring error.

Specimen preparation

It is difficult to machine microgrooves on the inner surface of pipeline restricted by processing conditions, so the drag reduction characteristic of pipeline outer surface with microgrooves in concentric annulus flow was tested only. The outer diameter of the scaled pipeline is 19.5 mm, the inner diameter of the scaled pipeline is 35 mm, as shown in Figure 7(a). Based on the optional microgrooves geometric parameters obtained by the numerical simulation, microgrooves were manufactured on the outer

surface of the aluminum pipeline by lathe machining, as shown in Figure 7(b). The height and width of microgroove can be controlled by the shape of lathe tool, the distance between grooves can be controlled by screw pitch. The micromorphology of microgrooves is illustrated in Figure 7(c).

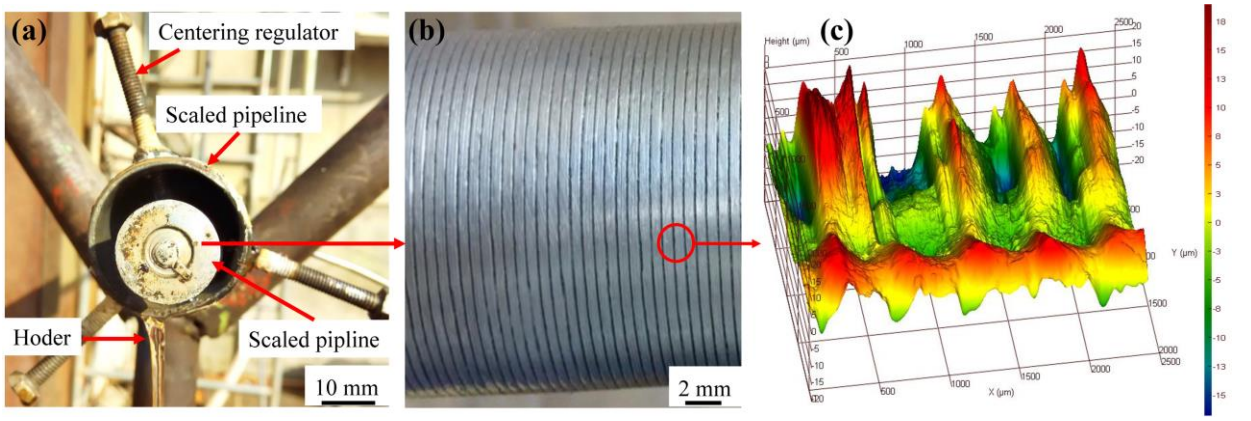

Figure 7: Specimen. (a) Scaled and (b) grooved pipeline in concentric annulus flow. (c) Micromorphology of microgrooves.

Validation of experimental repeatability and accuracy

Firstly, three repeated experiments were carried out under the same conditions to verify the repeatability of the experimental method. As can be seen from Figure 8, the results of three repeated experiments are approximately consistent, and the standard deviation is acceptable compared to the magnitude of the pressure difference. Then, the measured pressure difference was compared with the result of numerical simulation under the same flow rate.

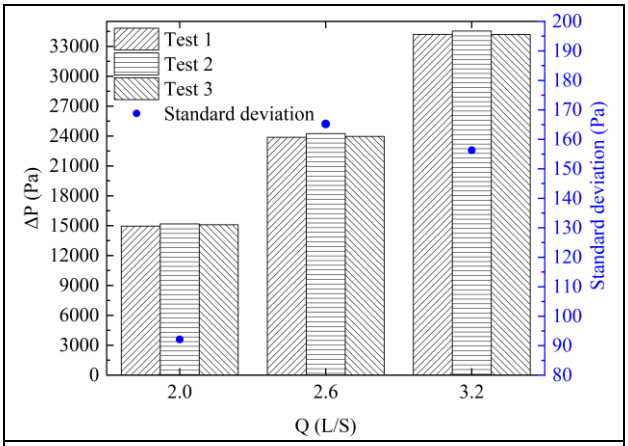

Figure 8: Comparison of repeated experimental results.

Figure 9 shows the comparison of simulation and experimental results, the maximum relative error is less than 2.0%, which can be acceptable. It can be concluded from the above analysis that the experimental method is accurate with good repeatability under different flow rates.

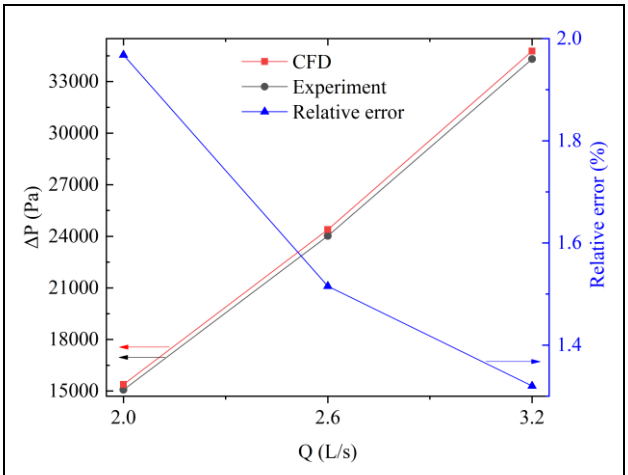

Figure 9: Comparison of CFD and experimental results.

Drag reduction evaluation method

Under the same experimental conditions, the average frictional head loss of the smooth pipeline and the bionic pipeline were compared to obtain the DRR of pipeline with transverse microgrooves, which can be defined as follows:

$$\eta = \frac{\lambda_s - \lambda_b}{\lambda_s} \times 100\% \qquad (14)$$

Where λ_s and λ_b are the friction loss factors of smooth pipeline and bionic pipeline, respectively.

The frictional head loss of smooth pipeline and bionic pipeline can be calculated by the following equations:

Smooth pipeline: $H_f = \frac{\Delta P_s}{\gamma} = \lambda_s \frac{L}{D} \frac{{U_s}^2}{2g}$ (15)

Bionic pipeline: $h_f = \frac{\Delta P_b}{\gamma} = \lambda_b \frac{L}{D} \frac{{U_b}^2}{2g}$ (16)

Flow rate: $Q = \frac{1}{4}\pi D^2 U$ (17)

Substituting Eqs. (15)-(17) into Eq. (14), the DRR of bionic pipeline can be obtained:

$$\eta = (1 - \frac{\Delta P_b}{\Delta P_s} \frac{{Q_s}^2}{{Q_b}^2}) \times 100\% \qquad (18)$$

Where Q is flow rate (L/s); ΔP_s, and ΔP_b are the pressure difference of smooth pipeline and bionic pipeline (Pa), respectively; L is the length of the test section (m); γ is the the unit weight of water (N/m^3). When the DRR is positive, it indicates that the transverse microgrooves have drag reduction effect in concentric annulus flow.

Results and Discussion

Single factor sensitivity analysis of groove geometric parameters

As shown in Figure 2, groove height h; groove width w and distance between grooves d are three significant geometric parameters of microgrooves, which determine the drag reduction effect of transverse microgrooves. The influence of microgroove geometric parameters on drag reduction performance was analyzed by single factor analysis method.

Microgroove height

Firstly, values of w = 0.2 mm, d = 1 mm, Re = 50000 keep constant, the flow drag and DRR of grooves with different heights in the pipe and annulus flow are shown in Figure 10(a, b), respectively. From Figure 10(a, b), the transverse microgrooves have advantage and disadvantage for flow drag. The decreasing of viscous drag is beneficial to achieve an effective DRR, while extra pressure drag is detrimental to the drag reduction performance. When the reduction of viscous drag is greater than the increase of pressure drag, the microgrooves have a drag reduction effect. The groove height has the same influence rule on the drag in the pipe and annulus flow: the pressure drag increases with the increase of height, the DRR first increases then decreases as the height increases. At the same time, the DRR of the annulus flow is lower than that of the pipe flow, because the microgrooves can only affect the inner wall of the annulus.

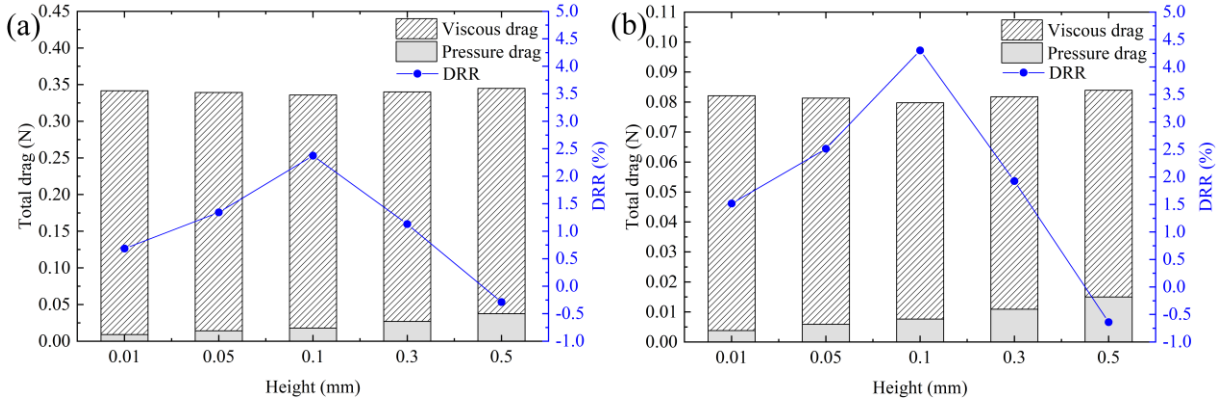

Figure 10: Effect of height on drag in (a) pipe flow and (b) annulus flow.

Microgroove width

Secondly, value of h = 0.1 mm, d = 1 mm, Re = 50000 keep constant. The flow drag

and DRR of grooves with different widths in the pipe and annulus flow are shown in Figure 11(a, b), respectively. From Figure 11(a, b), the groove width also has the same influence rule on the drag in the pipe and annulus flow: the pressure drag increases with the increase of width and the DRR first increases then decreases as the width increases.

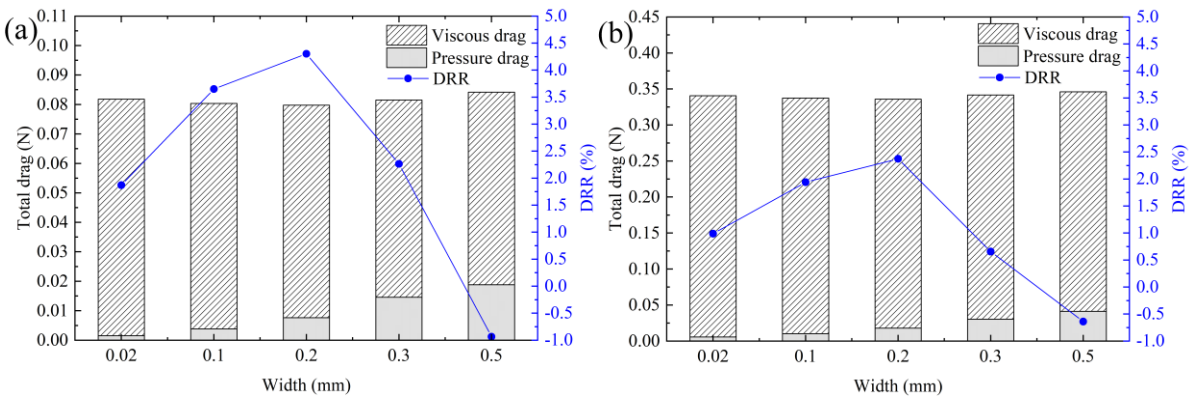

Figure 11: Effect of width on drag in (a) pipe flow and (b) annulus flow.

Distance between microgrooves

Finally, values of h = 0.1 mm, w = 0.2 mm, Re = 50000 keep constant. The flow drag and DRR of grooves with different distances in the pipe and annulus flow are shown in Figure 12(a, b), respectively. From Figure 12(a, b), the grooves distance also has the same influence rule on the drag in the pipe and annulus flow: the pressure drag decreases with the increase of distance. Meanwhile, the viscous drag increases as the distance increases, which led to the DRR first increases then decreases with an increase in the distance.

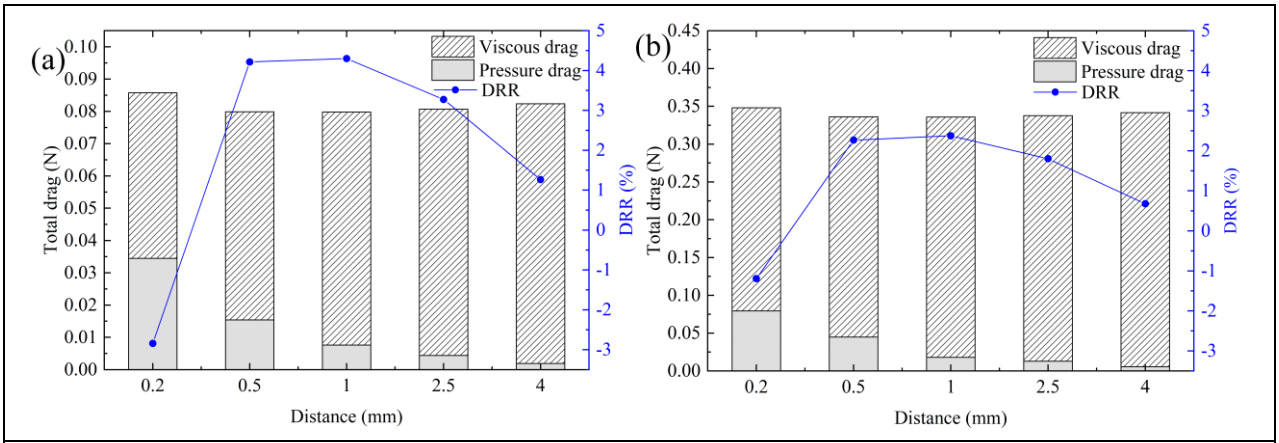

Figure 12: Effect of distance on drag in (a) pipe flow and (b) annulus flow.

Microgroove geometric parameters optimization

The geometric parameters of groove have a significant effect on drag reduction performance based on the analysis of single factor. It is necessary to optimize the parameters to further improve the DRR of grooves. In order to investigate the interaction between height, width and distance of grooves on the drag reduction effect and select the optimal parameters, orthogonal table of $L_9(3^4)$ was adopted for simulation parameters design (as shown in Table 2). The simulation results were processed by an intuitive analysis method with the DRR as the evaluation index.

Table 2 Grooves parameters optimization with orthogonal analysis in pipe flow.

Specimen	Factor A	Factor B	Factor C	Evaluation index
	Height(mm)	Width(mm)	Distance(mm)	DRR(%)
1	0.05	0.1	0.5	4.03
2	0.05	0.15	1	5.78
3	0.05	0.2	2	4.55
4	0.1	0.1	1	4.84
5	0.1	0.15	2	5.62
6	0.1	0.2	0.5	4.40
7	0.15	0.1	2	2.69
8	0.15	0.15	0.5	3.89
9	0.15	0.2	1	3.56

	k_1	4.787	3.853	4.107	
Level	k_2	4.953	5.097	4.727	
	k_3	3.380	4.170	4.287	
Range		1.573	1.244	0.620	
Optimal parameters		0.1	0.15	1	6.26

Table 2 shows the detailed simulation parameters and orthogonal analysis results of the pipe flow at a flow velocity of 5 m/s. The primary and secondary order of effect on DRR is height, width and distance, the optimal microgroove parameters are: h = 0.1 mm, w = 0.15 mm, d = 1 mm. In addition, the maximum DRR of 6.26% is achieved under the optimal microgroove parameters.

By using the same method, orthogonal simulated calculations were carried out under different velocities both in the pipe and annulus flow. Figure 13 shows the DRR of different specimens at the flow velocity of 1 m/s, 5 m/s, 10 m/s, respectively. From Figure. 13, the flow velocity has the same influence rule on the DRR of specimens in the pipe and annulus flow. At low velocity, the influence of microgroove parameters on DRR is slight; with the increase of flow velocity, the DRR of each specimen is significantly different. That is to say, as the Reynolds number increases, the influence of microgroove parameters on drag reduction becomes more sensitive to the effect of drag reduction owing to the thickness of near wall viscous sublayer decreases.

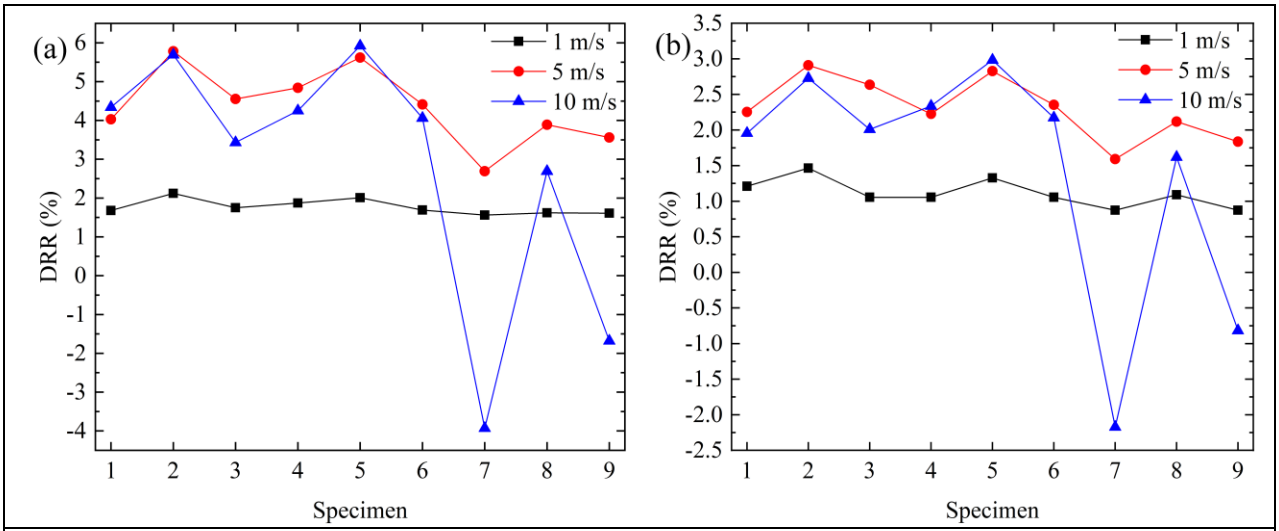

Figure 13: DRR of different specimens versus Velocity in (a) pipe flow and (b) annulus flow.

As shown in Table 3, the primary and secondary order of geometric parameters in the pipe and annulus flow are the same, which also keep the same at different flow velocities. The optimal parameters, however, change slightly at the velocity of 10 m/s. As the increase of velocity, the optimal width decreases, which is beneficial for entrapping the vortexes in the microgrooves.

Table 3 Orthogonal test range analysis results.

Velocity (m/s)	Primary and secondary order		Optimal parameters	
	Pipe flow	Annulus flow	Pipe flow	Annulus flow
1	A>B>C	A>B>C	$A_2B_2C_2$	$A_2B_2C_2$
5	A>B>C	A>B>C	$A_2B_2C_2$	$A_2B_2C_2$
10	A>B>C	A>B>C	$A_2B_1C_2$	$A_2B_1C_2$

Effect of Reynolds number on drag reduction in annulus flow

It was found that the flow velocity has a significant effect on the drag reduction and the same influence rule on the pipe and annulus flow from the study above section. Therefore, the change rule of DRR of bionic pipeline with optimal microgroove parameters was only analyzed in the annulus flow under a broader range of Reynolds number.

Figure 14 shows the influence of Reynolds number on the DRR and the ratio of pressure drag to the total drag. From Figure 14, the DRR first increases then decreases with the increase of Reynolds number, the bionic pipeline obtains a maximum DRR of 3.84% when the Reynolds number is 83500. At low Reynolds number, stable vortexes cannot be formed in the microgroove due to lack of energy, which is a crucial factor for drag reduction, resulting in the transverse microgrooves increase drag slightly. In addition, the ratio of pressure drag to total drag increases rapidly as the increase of Reynolds number. Therefore, with the increase of flow velocity, the increase of pressure drag will exceed the reduction of viscous drag, and the microgrooves would lose drag reduction effect eventually.

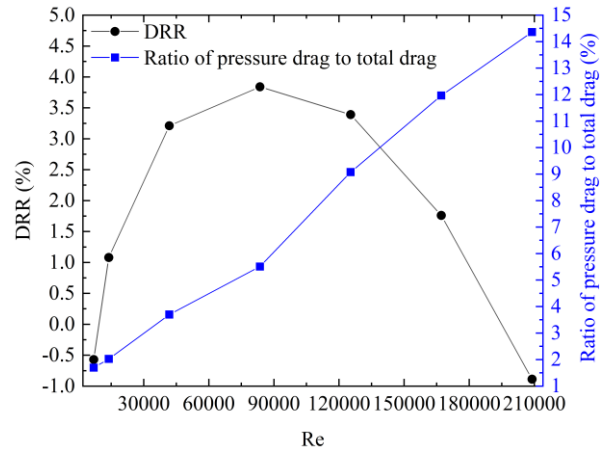

Figure 14: DRR and ratio of pressure drag to total drag versus Re in annulus flow.

Experimental validation of microgroove drag reduction performance

In the experimental study, microstructures were machined on the outer surface of the scaled pipeline with optimal microgroove parameters obtained in the numerical simulation. Then the frictional drag coefficient of bionic pipeline was compared with

that of smooth pipeline in the annulus flow under different flow rates. The change rule of DRR of bionic pipeline versus flow rate is plotted in Figure 15, which shows good agreement with the simulation results. The DRR first increases then decrease with the increase of flow rate, and the bionic pipeline has a drag reduction effect within a certain flow rate range. The maximum DRR is 3.21% at a flow rate of 2.4 L/s, which is lower than that obtained in the numerical simulation. The difference in results is mainly caused by machining error. As illustrated in Figure 7(c), it is inevitable to produce some small burrs around the microgrooves in the machining process, which is limited by processing accuracy and processing conditions. As a result, the drag reduction performance of transverse microgrooves has been verified by simulation and experiment. The Reynolds number for drag reduction effect is approximately 15000 - 90000. Therefore, it is theoretically feasible to reduce the pressure loss in the fluid transport by bionic pipelines.

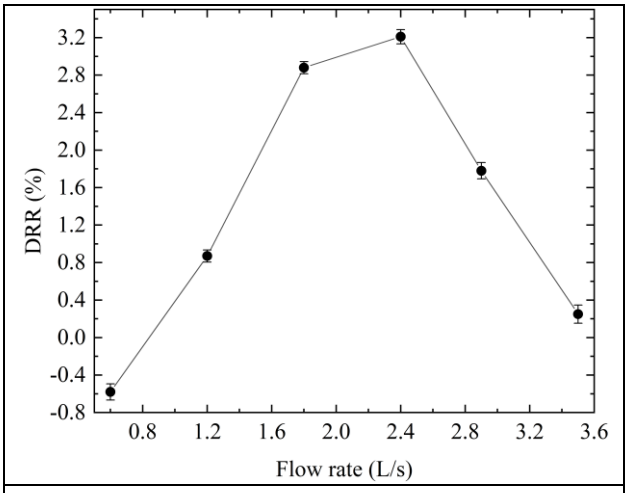

Figure 15: Influence of flow rate on DRR.

Flow field characteristics and drag reduction mechanism

This section takes pipe flow as an example, the drag reduction mechanism is

discussed by comparing the flow field characteristics of smooth pipeline and bionic pipeline with optimal microgroove parameters at a flow velocity of 8 m/s.

Flow field characteristics analysis

(1) Pressure drag

The pressure distribution of the near wall is illustrated in Figure 16, revealing the reason for the extra pressure drag induced by microgrooves. As shown in Figure 16, a local high-pressure zone is formed on the windward of the microgroove, and a local low-pressure zone is formed on the leeward of the microgroove. It is the adverse pressure gradient that causes the pressure drag, which is not conducive to drag reduction.

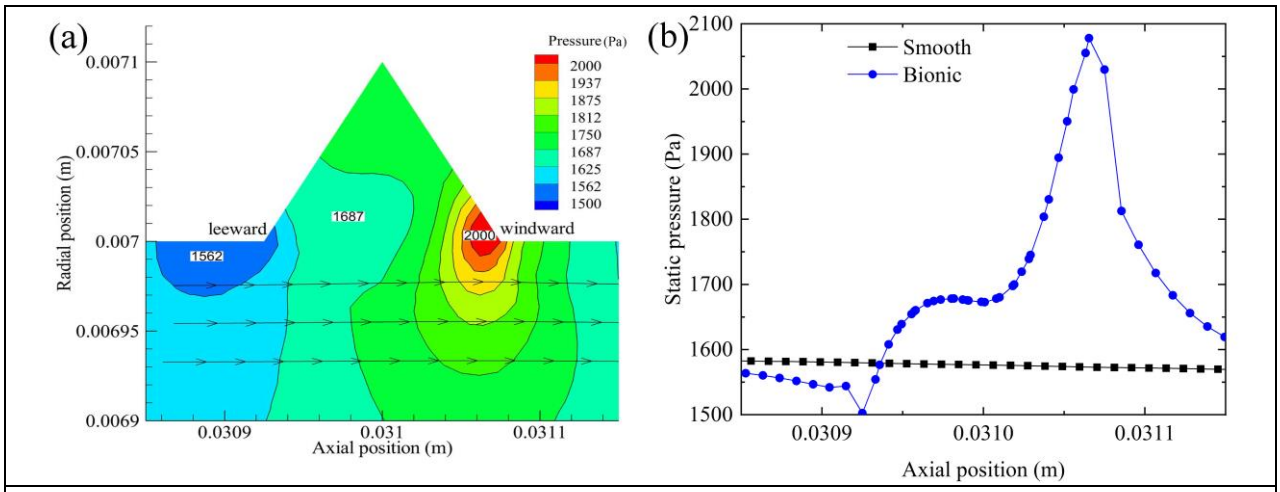

Figure 16: Pressure distribution. (a) Pressure contour of the near groove. (b) Pressure curve at the wall.

(2) Shear stress

Figure 17 depicts the wall shear stress of the smooth and bionic pipeline at the same axial position. From Figure 17, the shear stress of bionic pipeline first increases sharply on the windward of microgrooves, then descend quickly, finally lower than that of

smooth pipeline. In addition, the shear stress in the microgrooves is significantly reduced, forming a “low valley” on the curve. The mean shear stress of bionic surface is lower than that of smooth surface, which is the main reason for the reduction of viscous drag. Therefore, when the reduction of viscous drag is greater than the increase of pressure drag, the microgrooves have a drag reduction effect.

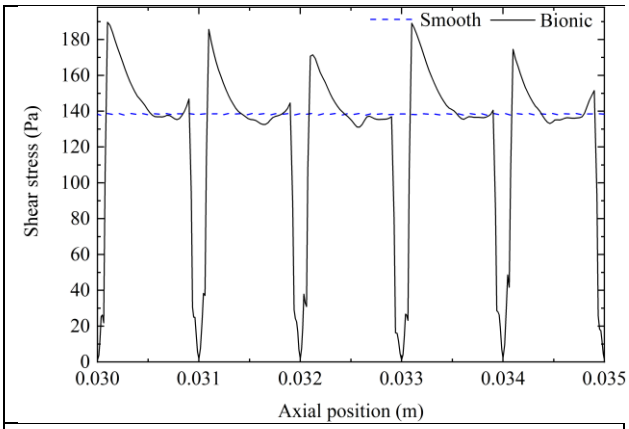

Figure 17: Wall shear stress of smooth and bionic pipeline.

(3) Turbulent intensity

Turbulent intensity is the ratio of turbulent fluctuating velocity to average velocity, which can intuitively reflect the magnitude of Reynolds stress. Figure 18 shows the distribution of turbulent intensity along the radial direction of the smooth and bionic pipeline flow field at the same axial position. As can be seen from Figure 18, the turbulent intensity of bionic pipeline in turbulent transition and core zones is lower than that of the smooth pipeline. Therefore, the transverse microgrooves can reduce the Reynolds stress to achieve a drag reduction effect.

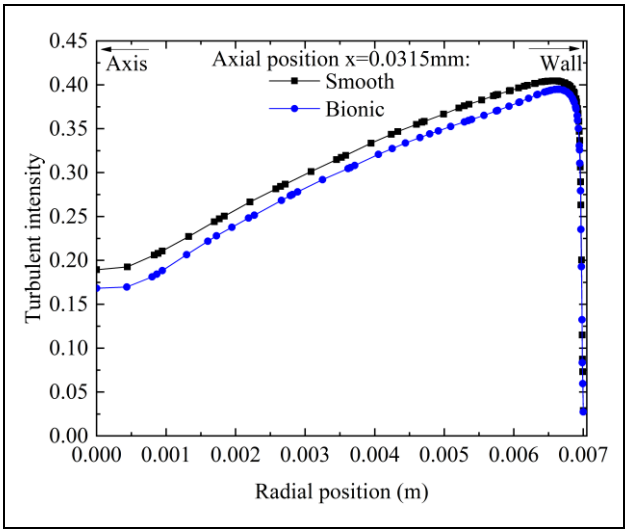

Figure 18: Distribution of turbulent intensity along the radial direction.

Drag reduction mechanism discussion

(1) Velocity distribution

As can be seen from the velocity contours in Figure 19, the boundary layer thickness of bionic surface is slightly increased compared with the smooth surface. Therefore, shear stress is reduced owing to the reduction of velocity gradient near the bionic surface. From Figure 19(b), low-speed micro-vortexes are formed in the microgroove due to the shear action of external fluids. Firstly, the micro-vortexes gather in the microgroove to form a “vortex cushioning effect”, liking a rolling bearing. Consequently, the external fluid flowing through the microgrooves did not contact the solid wall. The sliding friction between a solid and liquid interface in the smooth pipe flow is changed into rolling friction between a liquid and liquid interface in the bionic pipe flow. In addition, extra frictional drag is formed between the vortexes and grooved wall, whose direction is the same as the flow direction. Then the frictional drag has “driving effect” on fluid flow. The reduction of viscous drag is mainly caused by the above effects.

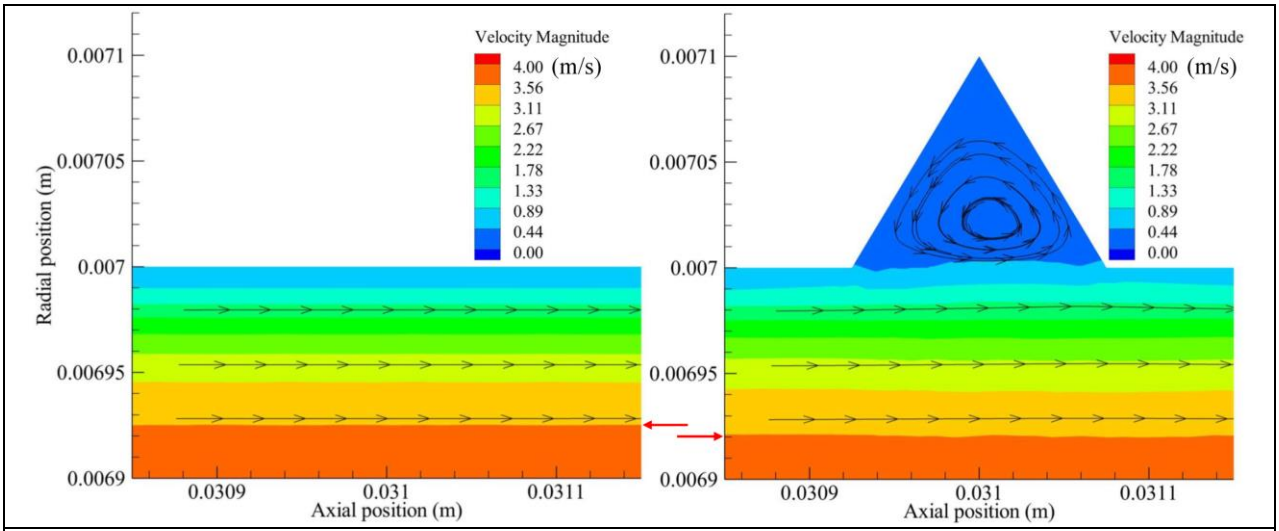

Figure 19: Velocity contour and streamlines near the (a) smooth surface and (b) bionic surface.

(2) Wettability

Jung et al. [40] found through experiments that microstructure with a higher contact angle provides a higher reduction of pressure drop in both laminar and turbulent water flows. Since surface wettability has significant influence on turbulent flow drag, the contact angle of experimental specimens was measured by the sessile drop method to investigate the impact of microgrooves on the wettability of pipeline surface. As shown in Figure 20, the contact angles are 68° and 99° on the smooth surface and bionic surface with microgrooves, respectively. In this case, the hydrophobicity of the pipeline surface is improved by the transverse microgrooves. The better the hydrophobicity of the surface, the lower the adhesion of the water. Therefore, the increased contact angle of bionic pipeline is beneficial to drag reduction.

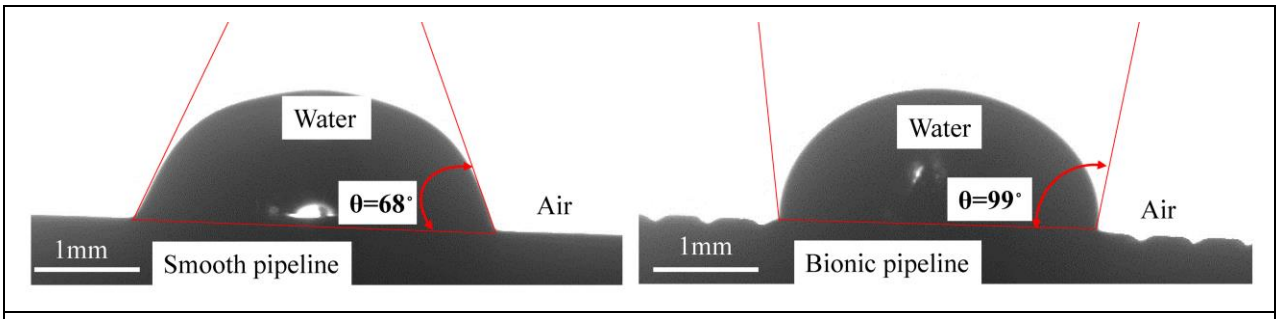

Figure 20: The profile of a droplet on the smooth and bionic surface.

Conclusions

In this study, the possibility of drag reduction of pipeline applied with bionic theory was investigated by numerical simulation and experimental methods. Besides the drag reduction mechanism of transverse microgrooves was revealed in terms of flow field characteristics and wettability. The following conclusions can be summarized.

(1) The transverse microgrooves have the same influence on the pipe and concentric annulus turbulent flow: reducing the viscous drag and inducing extra pressure drag. The DRR of the annulus flow is lower than that of the pipe flow under the same conditions.

(2) The drag reduction performance is significantly affected by the microgroove geometric parameters. The primary and secondary order of effect on DRR is height, width and distance, and the optimal parameters are: h = 0.1 mm, w = 0.15 mm, d = 1 mm. This conclusion is the same in the pipe and annulus flow.

(3) The pipeline with appropriate microgrooves has drag reduction effect under a certain flow rate, and a maximum DRR of 3.21% is achieved in the annulus flow experiment at a flow rate of 2.4 L/s.

(4) The CFD model predictions show a good agreement with experimental results in

terms of the influence rule of Reynolds number on DRR. The DRR first increases then decrease with the increase of Reynolds number. The Reynolds number for drag reduction effect is approximately 15000 – 90000. Therefore, it is theoretically feasible to reduce the pressure loss in the fluid transport by bionic pipelines.

(5) The drag reduction mechanism mainly attributed to the “vortex cushioning effect” and “driving effect” produced by the low-speed vortexes in the microgrooves. In addition, the hydrophobicity of the pipeline surface is improved by the transverse microgrooves, which can reduce the adhesion of water.

In the present study, the proposition of applying the bionic theory to the surface of the pipeline to reduce drag was verified from a theoretical perspective under ideal conditions. The influence of microgrooves on the strength of the pipeline, and the processing of bionic pipeline need to be further studied from the perspective of engineering application.

Acknowledgments

The authors gratefully acknowledge the financial support of the National Natural Science Foundation of China (Grant No. 51704323), and Natural Science Foundation of Shandong Province (Grant NO. ZR2017BEE053). This work is also supported by the Fundamental Research Funds for the Central Universities (18CX02177A), and National Basic Research Program of China (973 Program) (2015CB251202), China Scholarship Council (201806450092). The authors express their appreciation for the comments of the anonymous reviewers and the editors.

Nomenclature

τ	shear stress, Pa	y	normal distance from wall, m
μ	dynamic viscosity of fluid, $\mathrm{Pa}\cdot\mathrm{s}$	v	kinematic viscosity, m^2/s
du/dy	velocity gradient, 1/s	η	drag reduction rate, %
$\rho\overline{u_i'u_j'}$	Reynolds stress	F_s	average drag of smooth surface, N
ρ	density of fluid, kg/m^3	F_b	average drag of bionic surface, N
L	length of model, m	λ	friction loss factor
D	hydraulic diameter, m	ΔP	pressure difference, Pa
Re	Reynolds number	Q	flow rate, L/s
U_m	bulk velocity, m/s	γ	unit weight of water, N/m^3
f	viscous coefficient	h	height of microgroove, mm
u_τ	friction velocity, m/s	w	width of microgroove, mm
U	instantaneous velocity, m/s	d	distance between grooves, mm

References

[1] Herring H. *Energy,* **2006,** 31, 10-20.

[2] Hasan, S. W.; Ghannam, M. T.; Esmail, N. *Fuel,* **2010,** 89, 1095-1100.

[3] Chen, P.; Cheng, C.; Xin, J. In *Asia Pacific Drilling Technology Conference and Exhibition*, Tianjin, China, July 9-11, 2012; IADC/SPE 155826.

[4] Song, W.; Ni, H.; Wang, R.; Sun, B.; Shen, Z. *J. CO2 Util.* **2017,** 467-472.

[5] Meng, M.; Zamanipour, Z.; Miska, S.; Yu, M.; Ozbayoglu, E. M. *J. Pet. Sci. Eng.* **2019,** 172, 1077-1091.

[7] Kamel, A.; Shah, S. N. *J. Pet. Sci. Eng.* **2009,** 67, 23–33.

[8] Corredor, F. E. R.; Bizhani, M.; Kuru, E. *J. Fluids Eng.* **2015,** 137, 081103.

[9] Yang, S. Q.; Dou, G. *J Fluid Mech.* **2010,** 642, 279–294.

[10] Ceccio, S. L. *Annu. Rev. Fluid Mech.* **2010,** 42, 183-203.

[11] Martell, M. B.; Rothstein, J. *P. Phys Fluids,* **2010,** 22, 065102

[12] Gatti, D.; Cimarelli, A.; Hasegawa, Y.; Frohnapfel, B.; Quadrio, M. *J. Fluid Mech.* **2018,** 857, 345-373.

[13] Feng, B.; Chen, D.; Wang, J.; Yang, X. *Adv. Mech. Eng.* **2015,** 7, 849294.

[14] Li. K; Jing, D. Hu, J. Beilstein J. Nanotechnol. **2017,** 8, 2324-2338.

[15] Schneider, J.; Djamiykov, V.; Greiner, C. *Beilstein J. Nanotechnol.* **2018,** 9, 2561-2572.

[16] Li, D.; Guo, Z. *Appl. Surf. Sci.* **2018,** 443, 548-557.

[17] Baron, C. F.; Mimidis, A.; Puerto, D. *Beilstein J. Nanotechnol.* **2018,** 9, 2802-2812.

[18] Wen, L.; Weaver, J. C.; Lauder, G. V. *J. Exp. Biol.* **2014,** 217, 1656-1666.

[19] Bixler, G. D.; Bhushan, B. *J. Colloid Interface Sci.* **2013,** 393, 384-396.

[20] Etsion, I.; Kligerman, Y. *Trib. Trans.* **1999,** 42, 511-516.

[21] Ibatan, T.; Uddin, M. S.; Chowdhury, M. A. K. *Surf. Coat. Technol.* **2015,** 272, 102-120.

[22] Bixler, G. D.; Bhushan, B. *Adv. Funct. Mater.* **2013,** 23, 4507-4528.

[23] Liu, H.; Yang, Q.; Pei, X. *Acta. Pet. Sin.* **2016,** 37, 273-279.

[24] Meng, M.; Zamanipour, Z.; Miska, S.; Yu, M.; Ozbayoglu, E. M. *Rock Mech. & Rock Eng.* **2019,** 1-21

[25] Walsh, M. J. *AIAA J.* **1983,** 21, 485-486.

[26] Viswanath, P. R. *Prog. Aerosp. Sci.* **2002,** 38, 571-600.

[27] Dean, B.; Bhushan, B. *Phil. Trans. R. Soc. A.* **2010,** 368, 4775-4806.

[28] Rastegari, A.; Akhavan, R. *J. Fluid Mech.* **2018,** 838, 68-104.

[29] Bechert, D. W.; Bruse, M.; Hage, W. *Exp. Fluids.* **2000,** 28, 403-412.

[30] Zhang, D.; Luo, Y.; Xiang, L.; Chen, H. *J. Hydrodyn. Ser. B.* **2011,** 23, 204-211.

[31] Dean, B.; Bhushan, B. *Appl. Surf. Sci.* **2012,** 258, 3936-3947.

[32] Dai, W.; Alkahtani, M.; Hemmer, P. R.; Liang, H. *Friction*, **2018,** 1-10.

[33] Walsh, M. J. *AIAA J.* **1980.**

[34] Tokunaga, H. *In 37th Aerospace Sciences Meeting and Exhibit,* Reno, NV, January 11-14, 1999, 424.

[35] Dou, Z.; Wang, J.; Chen, D. *J. Bio. Eng.* **2012,** 9, 457-464.

[36] Mariotti, A.; Buresti, G.; Gaggini, G.; Salvetti, M. V. *J. Fluid Mech.* **2017,** 832, 514-

549.

[37] Eggles, J. G. M. Direct and large eddy simulation of turbulent flow in a cylindrical pipe geometry. Ph. D. Thesis, Delft University of Technology, Netherlands, 1994.

[38] Rahman, A.; Corredor, F. E. R.; Bizhani, M. In *ASME 2013 International Mechanical Engineering Congress and Exposition* California, USA, November 15-21, 2013; IMECE 65268.

[39] Chung, S. Y.; Rhee, G. H.; Sung, H. J. *Int. J. Heat Fluid Flow*, **2002,** 23, 426-440.

[40] Jung, Y. C.; Bhushan, B. *J. Phys. :Condens. Matter.* **2009,** 22, 035104.